Ultramicroscopy 165 (2016) 8–14

Contents lists available at ScienceDirect

Ultramicroscopy

journal homepage: www.elsevier.com/locate/ultramic

Full length article

Mapping the electrostatic potential of Au nanoparticles using hybrid electron holography

Cigdem Ozsoy-Keskinbora [a,*], Chris B. Boothroyd [b], Rafal E. Dunin-Borkowski [b], Peter A. van Aken [a], Christoph T. Koch [c]

[a] Stuttgart Center for Electron Microscopy, Max Planck Institute for Solid State Research, Heisenbergstr. 1, 70569 Stuttgart, Germany
[b] Ernst Ruska-Centre for Microscopy and Spectroscopy with Electrons and Peter Grünberg Institute, Forschungszentrum Jülich, 52425 Jülich, Germany
[c] Structure Research & Electron Microscopy group, Department of Physics, Humboldt University of Berlin, Newtonstraße 15, 12489 Berlin, Germany

ARTICLE INFO

Article history:
Received 16 June 2015
Received in revised form
18 March 2016
Accepted 23 March 2016
Available online 24 March 2016

Keywords:
Hybrid electron holography
Off-axis electron holography
In-line electron holography
Nanoparticles
Mean inner potential
High resolution phase retrieval

ABSTRACT

Electron holography is a powerful technique for characterizing electrostatic potentials, charge distributions, electric and magnetic fields, strain distributions and semiconductor dopant distributions with sub-nm spatial resolution. Mapping internal electrostatic and magnetic fields within nanoparticles and other low-dimensional materials by TEM requires both high spatial resolution and high phase sensitivity. Carrying out such an analysis fully quantitatively is even more challenging, since artefacts such as dynamical electron scattering may strongly affect the measurement. In-line electron holography, one of the variants of electron holography, features high phase sensitivity at high spatial frequencies, but suffers from inefficient phase recovery at low spatial frequencies. Off-axis electron holography, in contrast, can recover low spatial frequency phase information much more reliably, but is less effective in retrieving phase information at high spatial frequencies when compared to in-line holography. We investigate gold nanoparticles using hybrid electron holography at both atomic-resolution and intermediate magnification. Hybrid electron holography is a novel technique that synergistically combines off-axis and in-line electron holography, allowing the measurement of the complex wave function describing the scattered electrons with excellent signal-to-noise properties at both high and low spatial frequencies. The effect of dynamical electron scattering is minimized by beam tilt averaging.

1. Introduction

When investigating the atomic structures of nanoparticles, high-resolution TEM (HRTEM) is a widely applied method, in particular for the direct observation of surface structures, defects and interfaces [1–3], for which methods such as X-ray and neutron diffraction lack spatial resolution and single atom sensitivity. Even though a single HRTEM image may already provide valuable information about the atomic arrangement in a given sample, the information that it contains is either missing the phase of the electron wave (in an aberration-corrected HRTEM image) or it contains delocalized information that is not directly interpretable (if the image is not aberration-corrected and/or defocused). In both cases, only part of the information about the electron wave that has passed through the specimen is measured and the available information is often difficult to interpret [3]. Imaging an arrangement of atoms along a specific direction using electrons of a particular kinetic energy may produce many different images, depending on the aberrations of the imaging system. The complex-valued electron wave function at the exit face of the specimen, however, is independent of the imaging conditions and at large scattering angles generally contains information about the three-dimensional arrangement of the atoms that it has scattered from [4–6]. Multiple images that have been recorded at different planes of focus allow, in principle, the exit wave function to be recovered [7]. This so-called focal series reconstruction or in-line electron holography approach is one of many different forms of electron holography [8], a technique that was proposed by Dennis Gabor [9]. Starting from the reconstructed exit wave of the object, atomic positions, aberration-free images, electrostatic potentials [10], electric and magnetic fields [11], strain [12–14] and dopant distributions [14,15] within a specimen can be determined at both high and low magnifications. The acquisition of a series of defocused images does not require any specialized equipment attached to an electron microscope. However, quantitative reconstruction requires sophisticated computer algorithms to solve a

Abbreviations: AuNPs, gold nanoparticles; TEM, transmission electron microscope; HRTEM, high-resolution transmission electron microscope; MIP, mean inner potential

* Corresponding author.
E-mail address: c.ozsoy@fkf.mpg.de (C. Ozsoy-Keskinbora).

http://dx.doi.org/10.1016/j.ultramic.2016.03.007

large system of non-linear equations. Spatial frequencies of the phase well below the lateral coherence length of the illuminating electron beam are only accessible (e.g., by solving the transport of intensity equation – TIE [16]) if the boundary conditions for the phase are known.

In contrast to in-line electron holography, off-axis electron holography, which was pioneered by Möllenstedt and Düker [17], requires a much simpler reconstruction scheme. However, an electron biprism (a very thin wire kept at a positive potential) has to be installed near an intermediate image plane of the microscope. Reconstruction can then be performed by linear Fourier filtering [18]. In off-axis electron holography, the attainable spatial resolution is limited by the fringe spacing, which in turn is related to the biprism potential and magnification defined by the projector lens system. In order to properly sample the interference fringes their spacing should be no finer than ~3 times the pixel size of the detector. In-line and off-axis electron holography are highly complementary in their capabilities. While off-axis electron holography can be used to recover all spatial frequencies with equal signal-to-noise properties, in-line electron holography is more efficient in recovering high spatial frequency components of the wave function, but it is less sensitive to low spatial frequencies of in the phase. Recovering both high and low spatial frequencies of the phase at atomic and intermediate magnifications is a fundamental challenge and very important for investigating the properties of nanoscale materials.

Gold nanoparticles (AuNPs) are among the most widely used and investigated metallic nanoparticles, Their unique properties and excellent stability [19], high biocompatibility [20] and size and shape dependent electronic and optical properties [21] make AuNPs very good candidates for applications in catalysis [22,23], cancer research [24,25], biosensing [26] and many other areas. In all of these applications, not only the sizes, shapes and structures of the nanoparticles, but also the presence of impurities and details of the electronic structure of both the bulk material and the nanoparticle surfaces are of high importance. With all these properties Au nanoparticles are important and challenging materials to study by electron holography.

Here, we demonstrate the applicability of our recently developed hybrid electron holography approach [27] to atomic resolution electron holographic imaging of Au nanoparticles. In addition to the very high spatial resolution and large field of view that are accessible using this technique, we extend the hybrid electron holography scheme at intermediate resolution by varying the illumination direction with defocus slightly. This approach results in excellent phase sensitivity at intermediate magnification for measuring the mean inner potential (MIP) of a AuNP if the specimen thickness is known, showing at the same time that this approach is also much less sensitive to dynamical diffraction effects than conventional off-axis electron holography. The linear encoding of the phase in this experimental setup guarantees the phase to be unique, without the need of assuming any boundary conditions for the phase at the perimeter of the sampled area. Off-axis holography thus offers a way to experimentally obtain the boundary conditions on the phase that would allow for unique phase retrieval by in-line holography. However, the phase recovered by the TIE is very sensitive to noise in the experimental data, even in the case of known boundary conditions. Off-axis holography thus also provides very important low spatial frequency information, in addition to the boundary conditions, that could otherwise not be recovered reliably. Furthermore, the effect of the number of iterations and noise on the low spatial frequency components in the phase are discussed.

2. Experimental details

We collected in-line and off-axis electron holograms of Au nanoparticles suspended on a C grid using an FEI Titan 80–300 TEM equipped with two electron biprisms. Round illumination was used for both in-line and off-axis electron holography, keeping the experimental setup as simple as possible. At intermediate magnification, an upper biprism voltage of 84.4 V was used for acquiring off-axis electron holograms. A focal series consisting of 13 images recorded at focal planes separated by 30 nm was acquired from the same area as the off-axis electron hologram. Along with the defocus, the beam tilt was changed in proportion to the defocus, spanning a tilt range of approximately 2 mrad between the first and the last image in the series. Both the off-axis and the in-line electron holograms were energy-filtered using a 10 eV energy-selecting slit. For high-resolution off-axis electron holography, a bottom biprism voltage of 97.4 V was used and a 13-member focal series was acquired using a 5 nm defocus step. In contrast to the medium resolution experiment, high-resolution electron holography was carried out without using energy filtering and without introducing beam tilt. At magnifications allowing atomic resolution, off-axis electron holograms was acquired using an exposure time of 3 s, while an exposure time of 1 s was used for each image in the focal series. At intermediate magnifications, off-axis electron holograms were acquired for 20 s while each image in the focal series was acquired using a 1 s exposure time. All images were recorded on a 2048×2048 pixel charge-coupled device (CCD) camera (Gatan, Inc.). For off-axis electron holography, the vacuum reference waves and line profiles of the interference fringe contrast are shown in Suppl. Fig. S1. Reconstruction of in-line and hybrid electron holograms was performed using full resolution wave reconstruction (FRWR) software [28], which takes into account the modulation transfer function (MTF) of the CCD camera, partial spatial coherence and defocus-induced image distortions. Off-axis electron holograms were reconstructed using HolograFree [29] software. The reconstructed phase and amplitude images were used for calculating the mean inner potential (MIP) according to the following expression [30].

$$\phi(x, y) = C_E V(x, y) t(x, y) \tag{1}$$

Here, C_E is an electron-energy-dependent interaction constant, which is given by the expression

$$C_E = \left(\frac{2\pi}{\lambda}\right)\left(\frac{E + E_0}{E(E+2E_0)}\right)$$

where λ, E and E_0 are the electron wavelength, kinetic energy and rest mass energy, respectively. The value of C_E is 6.53×10^6 rad V^{-1} m^{-1} at an accelerating voltage of 300 kV.

The specimen thickness t was obtained from the reconstructed amplitude images using the expression [31].

$$t/\lambda_{in} = -2 ln\, A_o/A_r$$

where A_o is the amplitude of the electron wave within the object and A_r is the mean amplitude within the vacuum area. The inelastic mean free path λ_{in} was calibrated (20.97 nm for off-axis and 29.91 nm for hybrid electron holography, respectively) by ensuring that the inferred specimen thickness t was equal to the thickness reconstructed from a tomographic tilt series (see the Supplementary information) in the middle of the sample.

3. Results and discussion

Reconstructed amplitude and phase images of the AuNPs, which were obtained at intermediate magnification using the

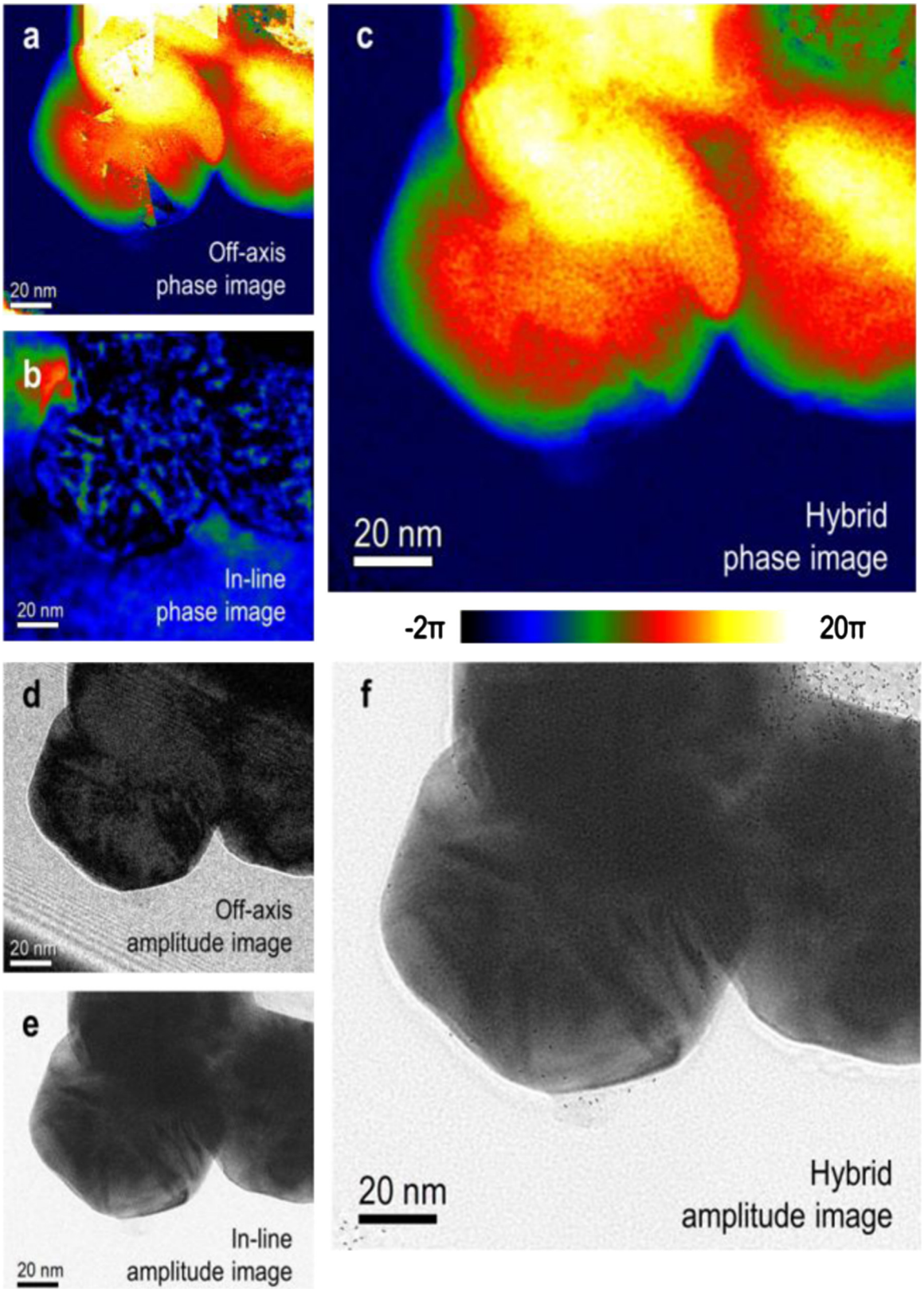

Fig. 1. (a, b, c) Phase and (d, e, f) amplitude of Au nanoparticles measured using off-axis, in-line and hybrid electron holography, respectively, at medium magnification.

three different electron holography methods (off-axis, in-line and hybrid electron holography) are shown in Fig. 1. Compared to the in-line electron holography phase image (Fig. 1b), which was reconstructed from 13 images, the hybrid electron holography approach, which combines information from both the off-axis electron hologram and the 13 defocused images, makes use of the low-spatial-frequency phase information in the off-axis electron hologram and thus recovers this contribution much better than in-line electron holography alone (Fig. 1c). The noise levels in both the amplitude and the phase are also much lower in the hybrid

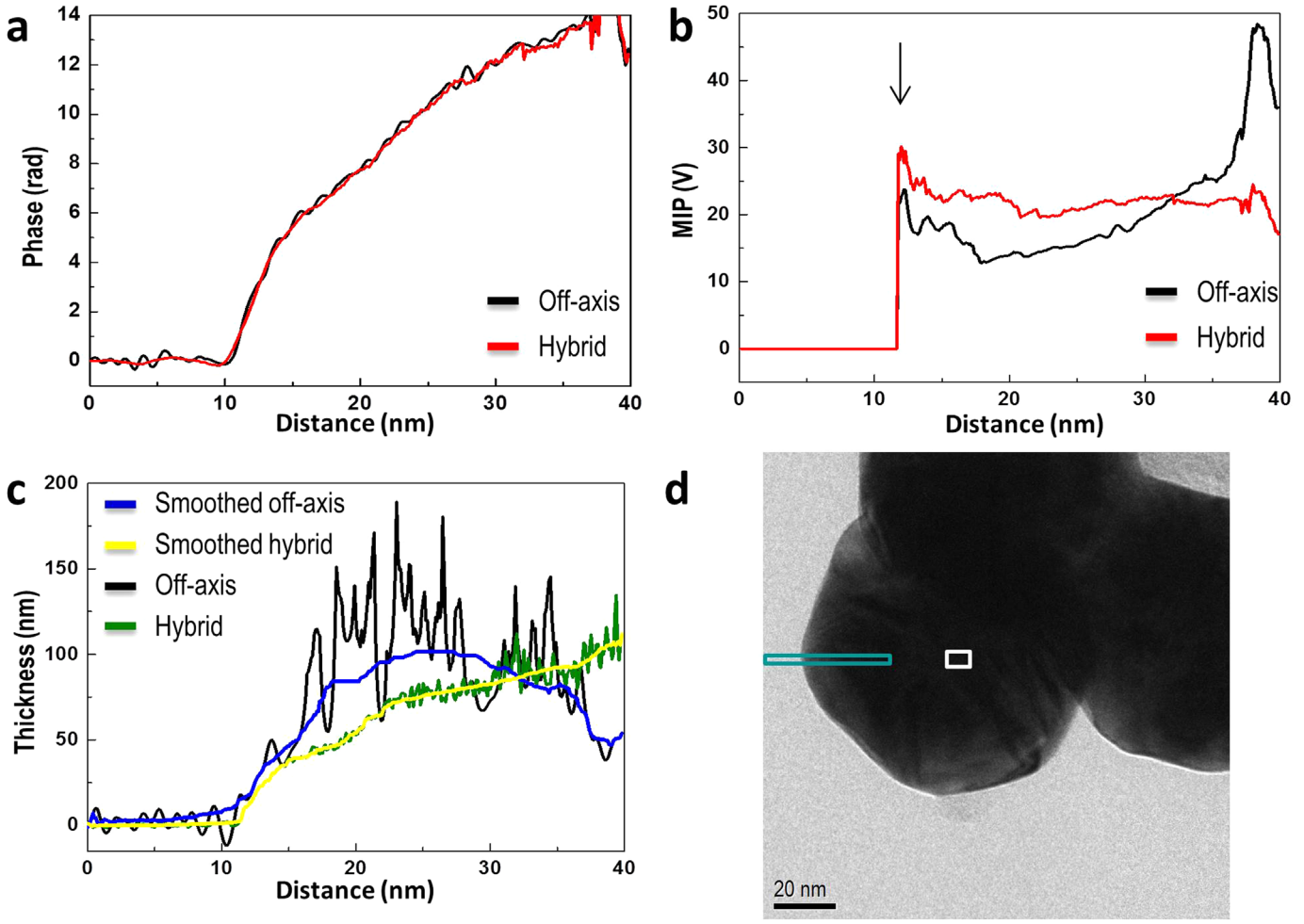

Fig. 2. (a) Phase and (b) MIP profiles obtained using off-axis and hybrid electron holography, respectively, from the region shown in (e) the black arrow in (b) indicates the edge of the specimen. (To the left of the arrow there is vacuum). (c) Specimen thickness profiles determined using the different techniques from the measured amplitude profiles. (d) Bright-field image showing the areas from which the profiles were extracted.

electron holography reconstruction than in the reconstruction from the off-axis electron hologram. Moreover, the hybrid reconstruction does not contain biprism fringe and unwrapping artefacts (see Suppl. Fig. S2), which are visible in the off-axis reconstruction (compare Fig. 1a, c, d and f.).

Experimental measurements of the MIP of gold in the literature vary between ~20 and 30 V [32–34], while calculated values vary between ~25.0 and 35.9 V [35,36]. The MIP values that we obtained are 23.16 ± 0.4 V from the off-axis electron hologram and 23.53 ± 0.12 V from hybrid electron holography when a sample thickness of 90 nm was assumed in the middle of the sample (see the selected area shown in Fig. 1a and c). Fig. 2b shows a line scan (the selected area shown in Fig. 2d) of the MIP calculated from the reconstructed phase and amplitude images for both the hybrid and the off-axis approach, according to Eq. (1). Although the phase (Fig. 1a) obtained using off-axis electron holography agrees, on average, with that obtained using the hybrid technique, the amplitude recovered from the off-axis electron hologram alone shows a strong influence from dynamical diffraction, leading to an apparent decrease in specimen thickness towards the center of the particle (see Fig. 2c). As each image in the focal series was acquired at a slightly different beam tilt (the total variation in beam tilt was ~2 mrad), each image was acquired at a slightly different dynamical diffraction condition. As the technique is designed to recover an electron wave function that best describes the intensity distribution in all of the images, the hybrid and in-line electron holography approaches effectively average over different dynamical diffraction conditions, reducing the influence of dynamical effects, resulting in more accurate amplitudes (Fig. 1e and f) and thickness maps. Fig. 2b shows that the inferred variations in MIP are much greater from off-axis electron holography alone than using the hybrid approach. Apart from surface effects, the MIP recovered using hybrid electron holography is almost constant, as would be expected. We therefore conclude that measuring the MIP of a strongly diffracting crystal using hybrid electron holography is more reliable than using off-axis electron holography alone. Fig. 2b also shows an increase in the MIP within a range of ~5 nm from the particle surface, Popescu et al. observed a similar increase in their 2007 work and attributed it to surface tension [32]. One of the advantages of off-axis electron holography is that the reconstructed amplitude and phase represent exactly the wave function of elastically scattered electrons, i.e, all inelastically scattered electrons have been removed. It is therefore expected that the elimination of the inelastic signal causes the amplitude determined from the off-axis electron hologram to be lower than that determined using in-line electron holography [37,38], since in the in-line and hybrid electron holography schemes inelastically scattered electrons can contribute to the recorded signal, so long as their energy loss is lower than the cut-off energy loss defined by the energy-selecting slit.

A significant advantage of hybrid electron holography over off-axis electron holography is its capability to record high-resolution

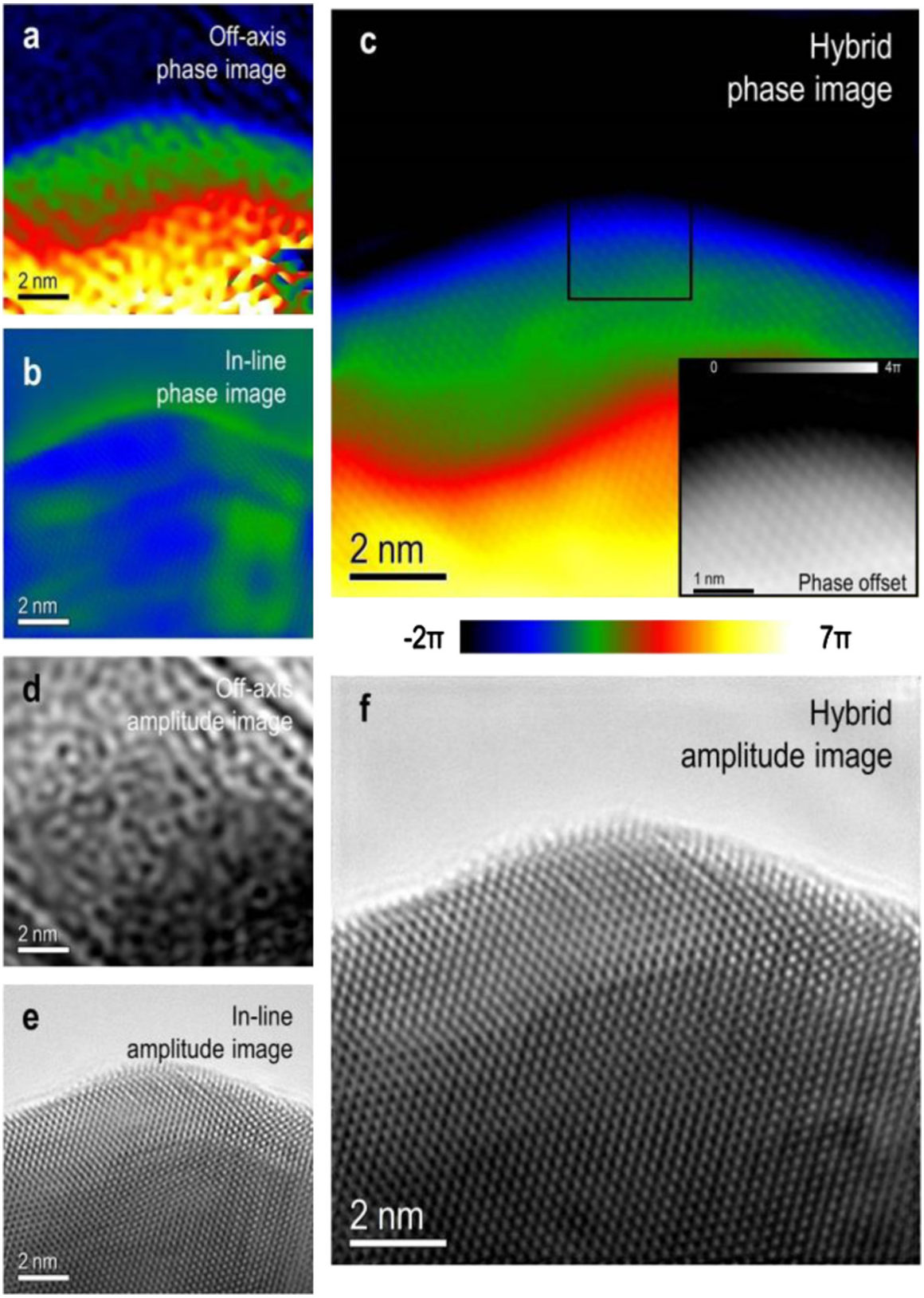

Fig. 3. (a, b, c) Phase and (d, e, f) amplitude measured using off-axis, in-line and hybrid electron holography, respectively, at atomic resolution.

electron holograms with a lower total electron dose and less stringent requirements on the experimental conditions, such as spatial coherence. The advantage of hybrid electron holography over pure in-line electron holography is that very low spatial frequencies in the phase are also recovered. Fig. 4 demonstrates the capability of hybrid electron holography (see Fig. 3c and f) to recover both low and high spatial frequency information with atomic resolution by utilizing a focal series of 13 images, which can in principle be reduced to as few as 3 images (Suppl. Fig. S3) for a reduced dose, although with less perfect results. The

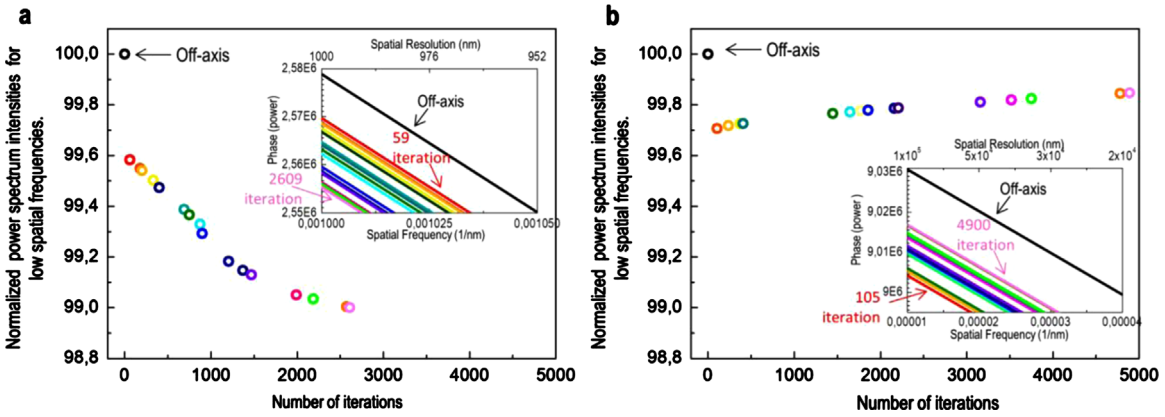

Fig. 4. Effect of the number of iterations on the low spatial frequencies of the phase. The normalized power spectrum intensities at a spatial frequency of 0.001025 nm^{-1} are shown as a function of iteration number (a) for a reconstruction from noisy data and (b) for a reconstruction from much less noisy data. The insets show the power spectra of the phase obtained by off-axis (black) and hybrid (different colors) electron holography for different numbers of iterations. (For interpretation of the references to color in this figure legend, the reader is referred to the web version of this article.)

recording of exit wave functions at high spatial resolution using off-axis electron holography alone is a very challenging task for reasons that are discussed in the literature [18,39], mostly because of requirements for long exposure times, very high stability of the instrument and sensitivity of the experimental setup to vibrations and stray fields, requiring a superior microscope and working environment. The degree to which off-axis electron holography results are impacted by non-ideal experimental conditions can be seen in Fig. 3a and d. In-line electron holography or focal series reconstruction is typically used when the main purpose of an experiment is to identify atomic positions, because accurate results at high spatial frequencies can be expected. However, variations in phase with characteristic spatial frequencies that are lower than the range of spatial frequencies that is reliably accessible using in-line electron holography cannot be quantified using this technique. This limitation becomes apparent in Figs. 1b and 3b, as the maximum phase shift expected from these materials is in the 10–15π range for intermediate magnifications and 7π for atomic magnifications according to more reliable off-axis values (Figs. 1a and 3a). However, the phase shift recovered from in-line electron holography is only $\pm 5\pi$ at intermediate magnifications and at atomic resolution only $\pm 1\pi$. In contrast, the phase recovered using hybrid electron holography contains both low and high spatial frequencies. The atomic structure can then be correlated directly with long-range electromagnetic fields associated with it.

In 2012 Ophus and Ewalds applied an iterative wave function reconstruction (IWFR) algorithm to perfectly coherent and noise free simulated data to point out how different spatial frequencies converge with the number of iterations and especially that the recovery of very low spatial frequency information in the phase required a very large number of iterations [40]. Under these conditions of perfect coherence the self-consistency in the data seems to encode the boundary conditions on the phase in the non-linear parts of the contrast. It is very unlikely that such conditions may be realized in a real experiment. The partial spatial coherence contribution to the transmission cross coefficient (TCC) very effectively dampens the very low spatial frequency information present in the wave function. At very low spatial frequencies the phase information theoretically still present in the image may thus be well below the noise level. Focal series data are thus generally not sensitive to very low spatial frequency phase information. Instead, noise is very likely to dictate the low spatial frequency information in phase images reconstructed from focal series. There is thus an open question as to how strongly the low spatial frequencies of the phase are affected by the number of iterations in our hybrid approach. To address this question, Fig. 4 shows the values of the lowest spatial frequency in the radially averaged power spectra of phase images obtained at different numbers of iterations of the hybrid holography approach normalized to the pure off-axis reconstruction (shown as 100%). Two different data sets, both acquired from Au nanoparticles, were used to observe the effect of low spatial frequency noise as well as the number of iterations. Fig. 4a shows the result from a hybrid electron holography data set, in which each of the defocused images had a different background due to random fluctuations of the energy filter. In the presence of such low spatial frequency noise, the hybrid electron holography low spatial frequency result diverges from the off-axis data with increasing iteration number. However it was also observed that the difference converged to about 1%. Fig. 4b is the result for the case of a homogeneous background. Here, the low spatial frequencies converge to the off-axis data when the iteration number increases. Contrary to the case presented in Fig. 4a, the hybrid and off-axis electron holography results show a better match at low spatial frequencies when the algorithm is kept running for more iterations when the noise is low (Fig. 4b). The differences between the off-axis and hybrid reconstruction have been reduced to 0.2% at 4900 iterations.

4. Conclusions

We have presented the first application of hybrid electron holography at atomic resolution. The primary advantage of the combined approach, which we apply to Au nanoparticles, is reliable reconstruction of the exit wave function with low noise across the complete range of spatial frequencies. Whereas atomic positions can be retrieved accurately from just the high spatial frequency components of the exit wave, the ability to record reliable measurements across the complete range of spatial frequencies becomes important for full quantification of, e.g., the relationship between structure and electrostatic or magnetic fields. We have also applied the technique at medium resolution, obtaining the mean inner potential of a Au nanoparticle and showing that varying the illumination direction with defocus reduces artifacts from dynamical scattering, in addition to yielding excellent signal-to-noise properties. Our measurements agree both with calculations [35,36] and with measurements reported using other techniques in the literature [32–34]. Both off-axis and hybrid electron holography show an increase in the measured MIP close to the edge of the specimen, as reported previously by others [32]. We have shown that feeding the in-line (focal series) reconstruction algorithm with off-axis data as an initial guess greatly enhances

the result at low spatial frequencies, with only minimal noise added at high spatial frequencies when compared to a pure in-line holography reconstruction (Fig. 3b, c, e and f). Finally, we presented an analysis of the effect of low spatial frequency noise on the convergence of the hybrid electron holography approach at low spatial frequencies from experimental data.

Contributions

COK made substantial contributions to the conception and design of the experiments and to the acquisition, analysis and interpretation of the data; CBB supervised and helped with experiments, in particular the off-axis holography; RDB supervised the off-axis holography experiments; PvA supervised the whole project and advised on the conceptual design; CK supplied the in-line electron holography reconstruction algorithm, supervised the overall study and helped with interpreting the data, drafting the article and revising it critically for important intellectual content.

Funding sources

CTK thanks the Carl Zeiss Foundation and the German Research Foundation (DFG, Grant no. KO 2911/7-1) for financial support. RDB thanks the European Research Council for an Advanced Grant no. 320832. The research leading to these results received funding from the European Union Seventh Framework Programme (FP7/2007-2013) under Grant agreement no. 312483 (ESTEEM2).

Acknowledgments

The authors gratefully thank John Bonevich for offering free public use of the HolograFREE off-axis holography reconstruction algorithm and Wilfried Sigle and Nahid Talabi for fruitful discussions and Luis M. Liz-Marzan and Cristina Fernandez-Lopez for providing samples.

Appendix A. Supplementary material

Supplementary data associated with this article can be found in the online version at http://dx.doi.org/10.1016/j.ultramic.2016.03.007.

References

[1] J.M. Cowley, High resolution electron microscopy, Annu. Rev. Phys. Chem. 38 (1987) 57–88.
[2] J. Liu, High-resolution scanning electron microscopy, in: N. Yao, Z. Wang (Eds.), Handbook of Microscopy for Nanotechnology, Springer, US, 2005, pp. 325–359.
[3] A.I. Kirkland, R.R. Meyer, "Indirect" high-resolution transmission electron microscopy: aberration measurement and wavefunction reconstruction, Microsc. Microanal. 10 (2004) 401–413.
[4] C.T. Koch, Using dynamically scattered electrons for three-dimensional potential reconstruction, Acta Crystallogr. Sect. A 65 (2009) 364–370.
[5] W. Van den Broek, C.T. Koch, Method for retrieval of the three-dimensional object potential by inversion of dynamical electron scattering, Phys. Rev. Lett. 109 (2012) 245502.
[6] D. Van Dyck, F.-R. Chen, 'Big Bang' tomography as a new route to atomic-resolution electron tomography, Nature 486 (2012) 243–246.
[7] L.J. Allen, W. McBride, N.L. O'Leary, M.P. Oxley, Exit wave reconstruction at atomic resolution, Ultramicroscopy 100 (2004) 91–104.
[8] J.M. Cowley, Twenty forms of electron holography, Ultramicroscopy 41 (1992) 335–348.
[9] D. Gabor, A new microscopic principle, Nature 161 (1948) 777–778.
[10] W.D. Rau, P. Schwander, F.H. Baumann, W. Höppner, A. Ourmazd, Two-dimensional mapping of the electrostatic potential in transistors by electron holography, Phys. Rev. Lett. 82 (1999) 2614–2617.
[11] K. He, F.-X. Ma, C.-Y. Xu, J. Cumings, Mapping magnetic fields of Fe_3O_4 nanosphere assemblies by electron holography, J. Appl. Phys. 113 (2013) 17B528-517B528-523.
[12] M. Hÿtch, F. Houdellier, F. Hüe, E. Snoeck, Nanoscale holographic interferometry for strain measurements in electronic devices, Nature 453 (2008) 1086–1089.
[13] H. Rösner, C.T. Koch, G. Wilde, Strain mapping along Al–Pb interfaces, Acta Mater. 58 (2010) 162–172.
[14] C.T. Koch, V.B. Özdöl, P.A. van Aken, An efficient, simple, and precise way to map strain with nanometer resolution in semiconductor devices, Appl. Phys. Lett. 96 (2010) 091901–091903.
[15] A.C. Twitchett-Harrison, T.J.V. Yates, S.B. Newcomb, R.E. Dunin-Borkowski, P. A. Midgley, High-resolution three-dimensional mapping of semiconductor dopant potentials, Nano Lett. 7 (2007) 2020–2023.
[16] M. Reed Teague, Deterministic phase retrieval: a Green's function solution, J. Opt. Soc. Am. 73 (1983) 1434–1441.
[17] G. Möllenstedt, H. Düker, Fresnelscher Interferenzversuch mit einem Biprisma für Elektronenwellen, Die Naturwissenschaften 42 (1955) 41.
[18] H. Lichte, P. Formanek, A. Lenk, M. Linck, C. Matzeck, M. Lehmann, P. Simon, Electron holography: applications to materials questions, Annu. Rev. Mater. Res. 37 (2007) 539–588.
[19] M.-C. Daniel, D. Astruc, Gold nanoparticles: assembly, supramolecular chemistry, quantum-size-related properties, and applications toward biology, catalysis, and nanotechnology, Chem. Rev. 104 (2003) 293–346.
[20] U. Saxena, P. Goswami, Electrical and optical properties of gold nanoparticles: applications in gold nanoparticles-cholesterol oxidase integrated systems for cholesterol sensing, J. Nanopart. Res. 14 (2012) 1–11.
[21] T. Jennings, G. Strouse, Past, present, and future of gold nanoparticles, in: W. W. Chan (Ed.), Bio-Applications of Nanoparticles, Springer, New York, 2007, pp. 34–47.
[22] B. Hvolbæk, T.V.W. Janssens, B.S. Clausen, H. Falsig, C.H. Christensen, J. K. Nørskov, Catalytic activity of Au nanoparticles, Nano Today 2 (2007) 14–18.
[23] S. Ichikawa, K. Okazaki, T. Akita, M. Okumura, K. Tanaka, M. Kohyama, Atomic and electronic structures of nano-interface In Au/TiO_2 catalyst – electron microscopic approach, MRS Online Proc. Libr. 738 (2002).
[24] W. Cai, T. Gao, H. Hong, J. Sun, Applications of gold nanoparticles in cancer nanotechnology, Nanotechnol. Sci. Appl. 2008 (2008) 17–32.
[25] J. Conde, F. Tian, Y. Hernández, C. Bao, D. Cui, K.-P. Janssen, M.R. Ibarra, P. V. Baptista, T. Stoeger, J.M. de la Fuente, In vivo tumor targeting via nanoparticle-mediated therapeutic siRNA coupled to inflammatory response in lung cancer mouse models, Biomaterials 34 (2013) 7744–7753.
[26] S. Guo, S. Dong, Biomolecule-nanoparticle hybrids for electrochemical biosensors, Trac. Trends Anal. Chem. 28 (2009) 96–109.
[27] C. Ozsoy-Keskinbora, C.B. Boothroyd, R.E. Dunin-Borkowski, P.A. van Aken, C. T. Koch, Hybridization approach to in-line and off-axis (electron) holography for superior resolution and phase sensitivity, Sci. Rep. 4 (2014) 7020.
[28] C.T. Koch, A flux-preserving non-linear inline holography reconstruction algorithm for partially coherent electrons, Ultramicroscopy 108 (2008) 141–150.
[29] J. Bonevich, HolograFREE software, in http://www.nist.gov/mml/msed/functional_nanostructure/electron_holography.cfm.
[30] D. Smith, M.R. McCartney, Practical electron holography, in: David C. Joy, Edgar Völkl (Eds.), Introduction to Electron Holography, Springer, US, 1999, pp. 87–106.
[31] M.R. McCartney, M. Gajdardziska-Josifovska, Absolute measurement of normalized thickness, t/λ_i, from off-axis electron holography, Ultramicroscopy 53 (1994) 283–289.
[32] R. Popescu, E. Müller, M. Wanner, D. Gerthsen, M. Schowalter, A. Rosenauer, A. Böttcher, D. Löffler, P. Weis, Increase of the mean inner Coulomb potential in Au clusters induced by surface tension and its implication for electron scattering, Phys. Rev. B 76 (2007) 235411.
[33] A. Goswami, N.D. Lisgarten, The measurement of inner potentials for copper, silver and gold, J. Phys. C: Solid State Phys. 15 (1982) 4217.
[34] S. Ichikawa, T. Akita, M. Okumura, M. Haruta, K. Tanaka, M. Kohyama, Electron holographic 3-D nano-analysis of Au/TiO_2 catalyst at interface, J. Electron Microsc. 52 (2003) 21–26.
[35] M. Schowalter, A. Rosenauer, D. Lamoen, P. Kruse, D. Gerthsen, Ab initio computation of the mean inner Coulomb potential of wurtzite-type semiconductors and gold, Appl. Phys. Lett. 88 (2006) 232108.
[36] A. Sanchez, M.A. Ochando, Calculation of the mean inner potential, J. Phys. C: Solid State Phys. 18 (1985) 33.
[37] A. Lubk, D. Wolf, H. Lichte, The effect of dynamical scattering in off-axis holographic mean inner potential and inelastic mean free path measurements, Ultramicroscopy 110 (2010) 438–446.
[38] C.B. Boothroyd, R.E. Dunin-Borkowski, The contribution of phonon scattering to high-resolution images measured by off-axis electron holography, Ultramicroscopy 98 (2004) 115–133.
[39] M. Linck, B. Freitag, S. Kujawa, M. Lehmann, T. Niermann, State of the art in atomic resolution off-axis electron holography, Ultramicroscopy 116 (2012) 13–23.
[40] C. Ophus, T. Ewalds, Guidelines for quantitative reconstruction of complex exit waves in HRTEM, Ultramicroscopy 113 (2012) 88–95.